Published in final edited form as:
J Comput Neurosci. 2011 August ; 31(1): 1–12. doi:10.1007/s10827-010-0293-9.

The impacts of geometry and binding on CaMKII diffusion and retention in dendritic spines

Michael J. Byrne, **M. Neal Waxham**, and **Yoshihisa Kubota**
Department of Neurobiology and Anatomy, University of Texas Medical School, 6431 Fannin, Houston, TX 77030, USA

Yoshihisa Kubota: Yoshihisa.Kubota@uth.tmc.edu

Abstract

We used a particle-based Monte Carlo simulation to dissect the regulatory mechanism of molecular translocation of CaMKII, a key regulator of neuronal synaptic function. Geometry was based upon measurements from EM reconstructions of dendrites in CA1 hippocampal pyramidal neurons. Three types of simulations were performed to investigate the effects of geometry and other mechanisms that control CaMKII translocation in and out of dendritic spines. First, the diffusional escape rate of CaMKII from model spines of varied morphologies was examined. Second, a postsynaptic density (PSD) was added to study the impact of binding sites on this escape rate. Third, translocation of CaMKII from dendrites and trapping in spines was investigated using a simulated dendrite. Based on diffusion alone, a spine of average dimensions had the ability to retain CaMKII for duration of ~4 s. However, binding sites mimicking those in the PSD controlled the residence time of CaMKII in a highly nonlinear manner. In addition, we observed that F-actin at the spine head/neck junction had a significant impact on CaMKII trapping in dendritic spines. We discuss these results in the context of possible mechanisms that may explain the experimental results that have shown extended accumulation of CaMKII in dendritic spines during synaptic plasticity and LTP induction.

Keywords

CaMKII; Diffusion; Translocation; Narrow escape problem

1 Introduction

CaMKII is a highly expressed protein in dendritic spines of CA1 hippocampal pyramidal neurons and is essential for the induction of long-term potentiation (LTP) (Lisman et al. 2002). LTP is correlated with an accumulation of CaMKII into dendritic spines in addition to basal concentrations that exist within the volume and at the postsynaptic density (PSD) (Merrill et al. 2005). During LTP induction, CaMKII undergoes a partial reversible translocation from the dendrite to accumulate in active spines. This translocation only occurs with spines experiencing Ca^{2+} influx through NMDA receptors (Lee et al. 2009). This spine specific accumulation persists for over an hour after LTP induction and possibly longer (Otmakhov et al. 2004). Translocation into the spine is believed to occur under diffusion

Correspondence to: Yoshihisa Kubota, Yoshihisa.Kubota@uth.tmc.edu.

Electronic supplementary material The online version of this article (doi:10.1007/s10827-010-0293-9) contains supplementary material, which is available to authorized users.

alone which begs the question: what are the mechanisms that control diffusion in a regulated and spine specific manner?

Dendritic spines are heterogeneously shaped structures with an average volume of 0.062 μm^3 that are connected to the dendrite through a narrow, roughly cylindrical neck (Harris and Stevens 1989). The rate of diffusional escape from spines through their narrow neck, which we call narrow escape rate, is one factor that regulates the retention time of CaMKII in dendritic spines. This narrow escape problem has been a subject of numerous theoretical studies and a series of mathematical formulae have been established (see Berezhkovskii et al. 2009 for overview). The time scale of this narrow escape rate is, however, ~ few seconds and is much shorter than the retention time of CaMKII observed by Otmakhov et al. (2004) and Yamagata et al. (2009). Other factors must act synergistically to retain CaMKII in dendritic spines in addition to spine morphology (the narrow escape rate). Furthermore, the spine morphology is not static and spine head volume shows a 50% increase during LTP induction via an F-actin-dependent dynamic process (Matsuzaki et al. 2004; Zhang et al. 2008). From these theoretical and experimental results, we believe there are three principle mechanisms that regulate diffusion and retention of CaMKII in the dendritic spines: spine morphology (narrow escape rate), F-actin complex at the base of the spine head and binding targets within the spines. In this study, we investigate the impact of each of these three factors independently and in combination on the relative rate of CaMKII diffusion and its retention in dendritic spines.

Translocation of CaMKII is specific to spines experiencing high Ca^{2+} influx through NMDA receptors (Lee et al. 2009). Neighboring non-stimulated spines do not show an increase in CaMKII concentration (Zhang et al. 2008; Lee et al. 2009). The mechanism that dictates this behavior is believed to be an F-actin complex that passively blocks the diffusion of large proteins in and out of the spine (Ouyang et al. 2005). This complex is regulated by βCaMKII that when binding Ca^{2+}/calmodulin, promotes the dissociation of βCaMKII from F-actin (Okamoto et al. 2007; Sanabria et al. 2009). This initiates a dynamic change in the F-actin complex and forms an enlargement pool of F-actin which is calmodulin dependent (Honkura et al. 2008). When jasplakinolide (a promoter of actin polymerization) is applied during LTP induction, the stable pool of F-actin blocks translocation of CaMKII suggesting that the F-actin complex is responsible for the block and that the destabilization of this complex allows diffusion (Ouyang et al. 2005). The required depolymerization of F-actin for translocation suggests that a steady-state increase in CaMKII due to increased PSD binding affinity is not sufficient to explain accumulation in a stimulated spine. Here, we examine a possible scenario that leads to the long retention of CaMKII in dendritic spines. First, even though the narrow escape time of CaMKII via diffusion is short (~ few seconds), it is long enough for CaMKII to explore the entire spine head and find high affinity binding sites before exiting from it. High affinity targets (e.g., at the post-synaptic density, PSD) may allow for short term accumulation of CaMKII as observed during LTP (~ few hundred seconds) and re-stabilization of the F-actin complex which in turn allows persistent accumulation.

In this paper we use the three dimensional simulator, Cellular Dynamic Simulator (CDS) (Byrne et al. 2010), to construct dendrite and spine morphologies to test these mechanisms. Pure diffusion is first examined to test CDS's algorithm and to gauge the mobility of CaMKII with or without obstacles. Second, the effects of spine geometry are explored by constructing various spine morphologies and determining their impacts on the narrow escape rate of CaMKII from dendritic spines. Then, we examine the retention time of CaMKII in dendritic spines by constructing a section of dendrite with numerous spines and by placing CaMKII in the dendrite and tracking a spine's ability to trap CaMKII. Third, the narrow escape problem is revisited by adding high-affinity CaMKII binding sites at the spine head

similar to a PSD to study the synergistic impact of binding on the narrow escape time (the retention time) of CaMKII with various morphologies of dendritic spines. Lastly, F-actin was added to the base of the spine head to test the ability of CaMKII to diffuse in and out of the spines when such structures block the neck. Note, a part of the first two issues have been studied by analytical methods (Dagdug et al. 2007; Berezhkovskii et al. 2009) but the last two issues cannot be addressed by pre-existing mathematical tools, which prompt us to investigate these issues by applying numerical methods.

2 Methods

2.1 Event-driven particle-based three-dimensional Monte Carlo simulation: Cellular Dynamics Simulator (CDS)

All simulations were performed using the Cellular Dynamic Simulator (CDS) (Byrne et al. 2010). The CDS is a novel particle-based, event-driven molecular collision and chemical reaction algorithmic scheme to simulate the impacts of stochasticity, volume-exclusion, and molecular crowding on cellular signaling systems. To simulate molecular diffusion in the cellular environment, one must take into account of the size of molecules (e.g., CaMKII) and also must calculate the exact timing of collisions between each pair of moving molecules (and between molecule and membrane) and execute these events one-by-one (while moving all molecules in the simulation simultaneously). In CDS, an event is anything that can occur in the simulation environment. As applied to the current study, these events include collisions, reactions and protein binding. When the first event occurs, the time is stored and then the algorithm searches for the next occurring event, then advances the simulation environment by that amount of time. That event is processed and the algorithm continues the loop, searching for the next event. Since CDS always searches for the first occurring event, no events are ever missed.

To calculate the exact timing of molecular collision, CDS relies on the first passage time principle while using discretized Brownian motion. At the beginning of each short time interval (dt), CDS generates random direction of movement for each diffusing molecule. From this direction of motion and from the diffusion coefficient of each molecule, CDS can detect all possible collisions between pairs of molecules and between molecules and static objects (i.e., membranes). If a collision is detected, CDS uses the first passage time principle to calculate the exact collision time τ ($0<\tau<dt$). CDS executes the earliest collision or other event (chemical reaction) one-by-one until time (dt), the pre-assigned “tentative” time interval. This event-driven scheme inspired by the first passage time theory is necessary to accurately calculate molecular collision in a crowded cellular environment and overcome the shortcoming of the pre-existing 3D Monte Carlo simulation algorithms (see Byrne et al. 2010 for more details). The short time interval (dt) used to generate random direction of movement is independent of the event driven algorithm. We confirmed that all simulation results in this work are accurate and independent of the choice of this short time interval (see below). (Fig. 1)

2.2 Morphology of dendrites and spines

Spine and dendrite geometry are defined as triangular meshes that are automatically generated in a CDS initialization tool based upon measurements from 3D EM reconstructions. Spines were represented as a spherical head attached to a cylindrical neck. These were automatically generated given three parameters: head radius, neck radius, and neck length (see Fig. 2(a)). In addition, we have analyzed the escape time of CaMKII with spine morphologies mimicking stubby and filopodial shapes (Section 3.2 and 3.4). CaMKII was represented as a sphere with a radius of 10 nm (Kolodziej et al. 2000) and a diffusion coefficient of 1.6 $\mu m^2 s^{-1}$ (Sanabria et al. 2008). The time step used for narrow escape

simulations was 10 μs and 50 μs for dendrite diffusion simulations. For each condition, we use the average of 5000 simulation runs. In all simulations presented here, we did not see any significant difference in the results between 10 μs and 50 μs (two-tailed *T*-test, $p<0.05$). Note that the mean squared displacement of CaMKII during this short time interval (10 μs) is smaller than the radius of CaMKII holoenzyme.

3 Results

3.1 The impact of obstacle binding (and transient anomalous sub-diffusion of CaMKII) in a simple environment

Molecular diffusion has been extensively modeled in a variety of cases including in unobstructed space, in the presence of obstacles and binding to obstacles (Saxton 1994; Saxton 1996). The microscopic geometry of the cellular interior or the extracellular environment or heterogeneous media (porous media) also has significant impacts of molecular diffusion and has been extensively studied (reviewed in Sykova and Nicholson 2008 and in Neuman and Tartakovsky 2009). Before analyzing the impacts of spine morphology and binding on CaMKII translocation in and out of the dendritic spines, we reexamine and confirm these theoretical studies using CaMKII and the CDS. The mean squared displacement ($<r^2>$) of a diffusing molecule in unobstructed space (normal diffusion) is proportional to time (Saxton 1994).

$$<r^2>=6Dt \quad (1)$$

Diffusion becomes sub-diffusive when $<r^2>$ is proportional to a power of time less than 1 ($=6Dt^a$, $a<1$). We study the impact of obstacles and binding by placing a single CaMKII randomly within infinite space. Obstacles added to the simulation space were placed on a regular three dimensional lattice with a separation of 20 nm (Fig. 1 (a)). These obstacles are immobile and have a radius of 2.5 nm (close to the size of smaller proteins such as calmodulin in CA1 spines). Each simulation was repeated 500 times. CaMKII diffusion was measured by recording distance relative to its starting position at 1 ms intervals for 1 s. Results are shown as a log plot where $<r^2>$ is divided by time. If $<r^2>$ is proportional to time as in Eq. (1), the result is a horizontal line indicating free diffusion. In fact, with no obstructions, the mean squared displacement divided by time should be equal to 6D, time-invariant constant, (Eq. (1)) (Fig. 1(b)). When obstructions were added, diffusion was reduced; however, the plot in Fig. 1(b) ("Obs.") is still a horizontal line indicating that the diffusion is not anomalous. Diffusion was reduced such that the average distance traveled by CaMKII in the presence of obstacles was 1.83 μm after 1 s as compared to 3.01 μm with no obstacles.

Another consideration to the hindrance of diffusion of CaMKII is the many binding targets within the dendritic spine. To test the effect of CaMKII target binding on apparent diffusion, binding sites were added to the immobile obstacles. Association to target occurred with a 10% probability upon collision of CaMKII and the target, equivalent to the macroscopic binding rate of 435 $\mu M^{-1}\ s^{-1}$ (see the section for binary chemical reactions in Byrne et al. 2009 for the method of calculating the macroscopic reaction rate from the microscopic reaction probability). This rate is within the typical range of association rate constants found in biochemical systems. In the bound state, CaMKII was immobile. Dissociation rates were set between $10^1\ s^{-1}$ and $10^5\ s^{-1}$ at order of magnitude intervals. When the diffusion becomes anomalous, the mean squared displacement divided by time is no longer a constant: it is a function of time. The deviation of this quantity, which we denote D(t), from the horizontal straight line indicates anomalous diffusion (the negative inclination of D(t) indicates anomalous sub-diffusion). CaMKII began to show anomalous diffusion (indicated

by a negative slope) with dissociation rates of 10^4 s^{-1}. However, D(t) relaxed back to a straight line after 500 ms for this dissociation rate. This anomalous diffusion was more pronounced with slower dissociation rates; however, for all cases tested here, the anomalous diffusion was transient (Fig. 1(b)). Therefore, the anomalous diffusion was transient as previously reported by Saxton (1996). The average distance travelled by CaMKII after 1 s was 1.13, 0.45, 0.15, 0.05 and 0.02 μm in order of fastest dissociation rate to slowest.

3.2 Escape from dendritic spines via diffusion (narrow escape problem)

CaMKII is surprisingly mobile given even in the presence of obstructions and binding with a dissociation rate of 10^3 s^{-1}: CaMKII was able to travel a distance of 150 nm over a 1 s time frame, for example. To test how spine morphology alone can retain such a fast diffusing protein, we calculated the escape time constant of CaMKII (i.e., the narrow escape time) to quantify how geometry of dendritic spines influences the mobility of CaMKII. Harris and Stevens (1989) provided detailed spine morphology from CA1 hippocampal pyramidal cells given in the form of head diameter, neck diameter and neck length. The range of generated geometry used in CDS was based upon the reported mean values plus and minus the standard deviation. Dimensions used to generate spines of various sizes were a neck radius of 50 to 100 nm (r_n), a neck length of 250 to 750 nm (L_n) and a head radius of 150 to 400 nm (r_h). Spine volumes ranged from 0.016 to 0.27 μm^3 (Fig. 2(a)). A single CaMKII was randomly placed in the spine head and an absorbing boundary was placed at the dendritic side of the neck that removed CaMKII from the simulation environment upon collision. Each simulation was repeated 500 times and for each trial the time when CaMKII exited the spine was recorded.

The decay of CaMKII out of the spine is well described by a single exponential curve as predicted by the pre-existing theory of the narrow escape problem (Fig. 2(b)) (see Berezhkovskii et al. 2009 and Biess et al. 2007 for reviews). In Fig. 2(c), the time constants of this exponential decay were plotted against the ratio between the volume of the head (V_h, as defined by the sphere) and the volume of the neck (V_n, as defined by the cylinder). The ratio will be referred to as V_h/V_n. This ratio was affected by the changes in any one of the three parameters used to generate the geometry of the spine. With L_n fixed, the narrow escape time is linearly proportional to the volume ratio (Fig. 2(c)). In fact, the narrow escape time from our simulation was well approximated by the formula given in Majewska et al. (2000).

$$\tau = \frac{L_n V_h}{\pi r_n{}^2 D} = \frac{L_n^2}{D}\frac{V_h}{\pi r_n^2 L_n} = \frac{L_n^2}{D}\frac{V_h}{V_n} \quad (2)$$

When the left-hand site of this formula (Eq. (2)) was compared against our simulation data, there was a 7.2 ± 1.2% difference on average. This approximation was one of four detailed in Berezhkovskii et al. (2009) and had the least error when compared to CDS results. The right-hand side of Eq. (2) confirms that the decay time and volume ratio (V_h/V_n) is proportional to the length of the neck squared divided by the diffusion coefficient. To check if the data produced by CDS also maintains this relationship, a linear regression was applied to each of the three data sets for different L_n (250, 500 and 750 nm). The slope of each fit differed from Eq. (2) by 5.4, −4.7 and −12.9% respectively which suggested that the theory allowed a reasonably close approximation to CDS results. The previous theoretical studies of narrow escape problems used “virtual” diffusing particles represented by points with zero size. When we compare our numerical simulations to the pre-existing formulae, we take into account the finite size of CaMKII and modify the neck and head radius in the previous mathematical formulae. However, still, the best fit was given by Eq. (2) by Majewska et al.

(2000). An important point to note is that some of the pre-existing theory relies on the singular perturbation concept to derive an explicit mathematical formula and the minor difference between numerical results and theory may still exist. The present work is not intended to systematically compare or re-examine these pre-existing mathematical formulae.

To reiterate, the CaMKII was modeled as a hard sphere with a radius set to 10 nm. It should be expected, as the radius of the neck approaches the radius of CaMKII, the theoretical narrow escape result described by Eq. (2) should break down and the contribution of r_n to the decay time should become dominant as the decay time becomes infinite. Does this breakdown occur for geometry in a physiological range of spine neck radii? To test the point of divergence from the theory, we generated several spine geometries with a r_n that varied from 15 to 40 nm, a fixed L_n of 500, and varied r_h such that the volume ratio remained constant (volume ratio chosen was that of an average spine). Neck radii of 40, 25 and 20 nm lead to a non-linear increase in decay time by 6.0, 48.9 and 153.9%, respectively. The average neck radius was 75±30 nm (sample of 100) and the minimum radius was 19 nm as reported by Harris and Stevens (1989). The majority of spines exist in a range applicable to traditional theory while several outliers may exhibit much stronger trapping characteristics.

Another possible situation in which Eq. (2) may fail to predict the narrow escape time is a spine with a wide neck. Such examples include stubby and filopodial shaped spines. To test the narrow escape problem in these spines, we created two morphologies within our current simulation scheme: a spine with a wide and relatively short neck (the head radius=251 nm, the neck radius=250 nm, and the neck length 250 nm) or a long cylindrical spine (the head radius=101 nm, the neck radius=100 nm, and the neck length 750 nm). We used these two morphologies to represent the stubby spine and the filopodial spine. For the stubby spine with a wide neck, we predict that the escape rate would be shorter than the narrow escape time predicated by Eq. (2). In fact, the simulated escape time is 0.008 s, much shorter than predicted by Eq. (2) (~0.053 s). As for the filopodial spine, we expect that the escape time is similar to or shorter than the time it takes for a diffusing molecule to travel from one end of the cylinder to the exit on the other side, i.e., $L_n^2/2D$ (see the first term in Eq. (3) in Berezhkovskii et al. 2009). The simulated escape time for the filopodial spine is 0.12 s, close to but shorter than the theoretical prediction ($0.18\text{s}=L_n^2/2D$). Thus, for all spine geometries tested here, the trapping time of CaMKII is close to or limited from above by the traditional theory.

3.3 Diffusion along dendrite with spines as transient traps

The impact of spine geometry was further examined by constructing the reverse case. CaMKII was placed in a section of dendrite and allowed to diffuse into and become trapped by spines. This type of problem is more relevant to biology when CaMKII in dendrites are recruited to the stimulated spine over the time scale much shorter than that due to protein synthesis. Trapping was examined by creating a section of dendrite 10 μm in length at a spine density of 2 μm^{-1} (Harris and Stevens 1989). Spines were generated in the same manner as in the narrow escape problem and were attached at random points about the cylindrical dendrite to achieve the desired density (Fig. 3(a)). The dendrite was defined as a cylinder with two radii used, 200 nm and 400 nm (approximate low and high range of measured dendrite radii). The boundary condition at the end of the neck was set as transparent such that diffusing molecules moved between the neck and dendritic compartment freely and unobstructed but the change of their locations was monitored by CDS. Simulations were run for 180 s and each simulation was repeated 10 to 100 times depending on the variability. The time step used here was 50 μs to speed up the simulation but no difference in dendrite diffusion was observed between 10 and 50 μs time steps.

For each simulation, 10 different environments were generated each with a random uniform distribution of spines (every spine had identical geometry for a given simulation). A single CaMKII was placed at the origin which was the center of the dendrite. The time that CaMKII spent in each visited spine was quantified by recording the instant of entrance and exit determined at the boundary of the dendrite and spine neck. The total time that CaMKII was trapped in the spines was divided by the number of times trapped to give the average amount of time trapped in a spine. This was plotted against the spine head to neck volume ratio used in the narrow escape problem. As seen, the average trapping time was proportional to the V_h/V_n ratio for a fixed L_n (Fig. 3(b)).

This simulation environment was also used to test if diffusion along the dendrite was free or anomalous. Santamaria et al. (2006) had simulated dendrite diffusion in Purkinje cells with spine densities ranging from 5 to 25 μm^{-1}. With these densities, they observed diffusion that was initially anomalous but relaxed back to normal diffusion within a short period of time. To test if the lower spine density in pyramidal neurons also results in anomalous diffusion, we extended our section of dendrite to 150 μm, used an average spine geometry (r_n=75, L_n=500, r_h=300), average dendrite radius (300 nm) and a spine density of 2 μm^{-1}. As a control, we created an equal section of dendrite but lacking spines. Diffusion in the control case was free (normal) (Fig. 3(c)). Diffusion in the case of spines was initially anomalous and became normal after ~20 s (the simulation was run to 180 s). Our results reproduce data from Santamaria et al. (2006) where given appropriate time, there exists a transition from anomalous to normal diffusion in spiny sections of dendrites.

3.4 Narrow escape problem with high affinity binding sites at PSD

Morphology alone had the ability to retain CaMKII for ~4 s given average spine dimensions (r_h =300 nm, r_n = 75 nm, L_n =500 nm) (Fig. 2). This is short compared to the experimentally observed duration of CaMKII accumulation following LTP induction (Otmakhov et al. 2004). Because CaMKII interacts with high affinity targets found in the PSD, we revisited the narrow escape problem and attached high affinity binding targets of CaMKII at the head of spine where a PSD is located. Even though we do not simulate or create PSD like structure, in what follows, we call this localized area of high affinity binding sites (collectively) “PSD”. To examine how effective the PSD was to the contribution of accumulation, CaMKII decay time out of the spine was measured with variable affinity to PSD binding targets.

The center of the PSD was placed opposite the neck entrance and a 100 nm radius section of this membrane was defined to be the PSD. The surface area of this region was approximately the PSD surface area reported by Harris and Stevens (1989). 50 generic binding targets were uniformly distributed on the PSD (Fig. 4(a)). We do not know an exact number of CaMKII binding sites in PSD. One major CaMKII binding target in the PSD are NMDA receptors (5~15 NMDA receptors per PSD) (Shen et al. 2000; Kalantzis et al. 2009) and CaMKII interacts with its subunit with different affinities (Leonard et al. 1999). Other proteins in PSDs that are also known to bind CaMKII include α-actinin and densin-180, among others (Walikonis et al. 2000; Strack et al. 2000). From such work, 50 binding sites seems a reasonable first approximation. The association probability of CaMKII upon collision was set at 100% (= the diffusion-limited) in order to assess the maximum impact of binding sites. Simulations were run with unbinding rates of 0.1 s^{-1}, 1 s^{-1}, 10^2 s^{-1} and 10^4 s^{-1} which bracketed a range of target affinities from high to low affinity binding. With relatively fast dissociation rates (10^2 s^{-1} and 10^4 s^{-1}), the decay time constants for the escape from spines were well approximated by a single exponential. We plot these decay time constants against V_h/V_n (Fig. 4(b)) as before. Decay time was proportional to the volume ratio, but on average with respect to the narrow escape problem, decay rates were 10.9% slower with 10^4 s^{-1} dissociation rate and 76.9% slower with 10^2 s^{-1} dissociation rate.

With higher target affinities (dissociation rates 1 and 0.1 s^{-1}), the CaMKII escape displayed different dynamics from lower target affinities and began to control the mode of CaMKII diffusion. The narrow escape process is no longer fit well by a single exponential decay. The decay of CaMKII in the spine head was fit with a double exponential and the amplitude of the slow decay was on average equal to that of the fast decay amplitude (Table 1). The slow exponential decay time, averaged for all geometries for the 1 s^{-1} dissociation rate, was 134.96 s and for the 0.1 s^{-1} rate was 1285.16 s (~21.4 min). The significant increases of the narrow escape time were also observed for the stubby spines (~ 418-fold increase) and the filopodial spines (~ 174-fold increase) with the high affinity binding sites (the dissociation rate 1 s^{-1}) (See Section 3.2 for their morphologies). While high affinity binding sites dramatically slowed down the narrow escape process, the geometry of the spines still had a significant impact but in a manner different from what we observed in Fig. 2. In high affinity cases, the theory described in Eq. (2) broke down and the linear relation between V_h/V_n and the narrow escape time was lost. The radius of the neck (r_n) became the primary morphologic factor determining decay time (Fig. 4(c)). A spine with a V_h/V_n three times greater had a decay time three times faster than a smaller spine, but the small spine had a r_n half that of the larger spine.

The synergistic effect of narrow escape rate and PSD binding was further tested with a spine that had a high affinity PSD, but without the narrow neck. An average spine was constructed with the exception that its neck radius was equal to the head radius forming a cylinder. 50 binding targets were added to the PSD with an unbinding rate of 0.1 s^{-1} and a single CaMKII was initialized to a target bound state (immobile) and the simulation was repeated 1000 times. The decay time of CaMKII out of the spine was 134.6 s. The identical scenario was recreated with the neck radius set to 75 nm. The decay time was 834.6 s, 6.2 times slower than with no narrow escape geometry imposed. Without the narrow neck, a single CaMKII on average would rebind to a PSD target 9.5 times after the initial dissociation. With the (narrow) 75 nm neck radius, the average number of target associations (including re-associations) was 51.7. Clearly, the confinement of CaMKII within the spine head compartment (due to the narrow escape geometry) increases the probability of recurrent binding of CaMKII to the PSD. This is consistent with our observation in Fig. 2(d): CaMKII extensively explores the entire compartment of spine head before exiting from it.

3.5 Confinement of CaMKII by F-actin

Although translocation of CaMKII during LTP occurs from the dendrite to the spine, to examine how effective a passive block of a F-actin complex is against CaMKII diffusion, the narrow escape rate was examined in the presence of F-actin at the spine neck-head boundary. A simple F-actin complex was created by placing cylindrical shaped F-actin in a parallel fashion across the base of the head with variable spacing. F-actin was generated simply as a cylinder with a diameter of 8 nm (Holmes et al. 1990; Ikawa et al. 2007). Spacing of F-actin was varied between 20.025 and 24 nm (a spacing of 20 nm resulted in a total block; data not shown). The spine morphology used was an average sized spine with a head radius of 250 nm, a neck radius of 75 nm and a neck length of 500 nm (Fig. 5(a)).

Spacing of F-actin acted as an effective gate for CaMKII diffusion that resulted in a switch between rapid diffusion out of the spine and blocked diffusion (Fig. 5(b)). Clamping the spacing down to 21 nm slowed the decay rate (2.37 s) by only double the control case (no F-actin). F-actin spacing of 20.2 nm showed a decay rate of 11.55 s. This decay was less than decay rate of the largest spine used in the narrow escape problem with geometry alone (14.02 s) (Fig. 2(c)). These results indicated that to passively block CaMKII diffusion effectively, F-actin must be tightly bundled. Interestingly, such tightly spaced and largely parallel actin bundles have been observed *in vitro* by Sanabria et al. (2009) via CaMKII/actin interactions.

Empirical data has shown that the half-maximal time for CaMKII translocation into a spine is ~20 s upon addition of glutamate (Shen and Meyer 1999). If a simulated section of dendrite had spines which obstructed CaMKII diffusion, and a single spine had the obstruction removed, what is the translocation time into that spine? To determine the accumulation time given a spine with an unobstructed neck, we used a 10 μm section of dendrite with a spine density of 2 μm^{-1}. The dendrite was populated with 0.5 μM of CaMKII and physical blocks were placed at the neck/head junction of all but one spine (Fig. 5(c)). The open spine had a PSD with 100 targets where association was diffusion limited and the dissociation rate was 1 s^{-1}. There was a maximum accumulation of 94.37 (1.32 μM) CaMKII and the half-maximal time to equilibrium was 7.25 s (Fig. 5(d)). We expected this result to be faster than experimental data as there was no obstruction between the neck and head for the duration of the simulation which allowed immediate CaMKII translocation into the spine. Physiologically, we hypothesize that there is a delay in breakup of the F-actin complex upon the addition or uncaging of glutamate at the spine. Ca^{2+} influx and subsequent binding to calmodulin provokes the dissociation of βCaMKII from F-actin, leaving the F-actin complex unbundled (Okamoto et al. 2007). The half maximal time for dissociation of βCaMKII from F-actin has been measured at 5 s upon addition of glutamate (Shen and Meyer 1999). This delay in the breakup of the F-actin complex may explain the time discrepancy between experimental data and our results.

4 Discussion

We have simulated various mechanisms that are required for CaMKII accumulation to show how, in concert, these mechanisms can contribute to the translocation of CaMKII into dendritic spines. CaMKII, despite its large size and slow diffusion coefficient, is highly mobile in the absence of crowding or protein-protein interactions. Regulation of its diffusion by three proposed mechanisms (synaptic morphology, binding sites in the PSD, and/or block by F-actin) may account for the experimentally observed translocation and accumulation of CaMKII within synaptic spines.

Spine morphology has been identified (or hypothesized) as a potential mechanism for trapping and localization of signaling molecules (Bloodgood and Sabatini 2005). Our results indicated that this may be misleading given the small duration of trapping (~4 s), even for large, slow diffusing proteins. Instead, the present work indicated that the direct effect of morphology was to retain diffusing molecules for adequate time as to be trapped by other mechanisms. If a single CaMKII was tracked during a narrow escape simulation, we observed that it quickly sampled the entire spine volume (Fig. 2(d)). With an average spine geometry and CaMKII placed at the center of the spine head, CaMKII took 1.58 s to explore the entire spine volume and 2.87 s to translocate to the dendrite. The short term effect of trapping would allow for CaMKII to enter and effectively explore the spine to locate potential targets prior to exiting out of the spine through the neck.

The postsynaptic density is a reasonable candidate for the long term accumulation of CaMKII given the abundance of high affinity targets found there. This accumulation is enhanced during the induction of LTP when CaMKII becomes Ca^{2+}/calmodulin bound or autophosphorylated at T286 leading to an increase in affinity to PSD targets (Merrill et al. 2005). However, spine morphology was essential for this long term accumulation in addition to high affinity targets in the spine by confining CaMKII and increasing the probability of binding (and rebinding) to the PSD. This is consistent with our finding in Fig. 2(d) that CaMKII extensively explores the entire spine head compartment before exiting from it. Under such a scenario, the high binding affinity of PSD associated targets will dramatically slow down the narrow escape process. The morphology alone could trap CaMKII for ~4 s and high affinity targets alone could trap for ~110 s, while the two combined trapped for

~588 s. With a high affinity binding sites at the PSD, the mode of CaMKII movement (diffusion) is different from the one when the spine head wall was completely reflective. As a result, the narrow escape time is now controlled by the radius of the spine neck (Fig. 4(c)).

CaMKII accumulation has been observed for durations of up to an hour after LTP induction (Otmakhov et al. 2004; Yamagata et al. 2009). The increased affinity to PSD targets due to autophosphorylation of CaMKII (Merrill et al. 2005) is essential to short term localization to the PSD. Dissociation of CaMKII-T286A (autophosphorylation-deficient mutant) from the PSD is significantly faster than for the wild-type enzyme (Shen and Meyer 1999). This suggests that increased affinity to PSD targets as a result of autophosphorylation may be essential for CaMKII localization to the PSD. However, with the highest binding affinity used in our simulations (22.16 nM), we showed that the CaMKII decay time out of the spine averaged ~20–30 min. One explanation for this discrepancy was that this affinity was less than the affinity for typical PSD targets (NR2B, Densin-180, PSD-95, etc.). The K_d value for CaMKII binding to target in an average sized spine was 22.16 nM given a dissociation rate of 0.1 s^{-1}. Strack and Colbran (1998) observed phosphorylated αCaMKII had a K_d value for binding to NR2B of ~150 nM which suggests that an appropriate dissociation rate may be between the two slowest used in the present study and a higher affinity may not be physiologically accurate. An alternative explanation for this discrepancy is that each CaMKII holoenzyme is composed of multiple subunits and each subunit may interact with multiple binding sites in the PSD simultaneously. Recent experimental data strongly suggests this scenario (Robison et al. 2005). Under such a multivalent interaction circumstance, the life time of CaMKII-PSD binding is much longer than predicted from the dissociation constant (Goldstein and Perelson 1984). In addition, the PSD is not the only place for binding sites for CaMKII. Actin filament and other molecules interact and bind CaMKII (Ohta et al. 1986). As shown in Fig. 1(b), the binding slows down the diffusion of CaMKII and transiently causes anomalous sub-diffusion of molecules. If again, CaMKII binds to these molecules via multiple binding sites, it may result in an extended trapping of CaMKII in the dendritic spines.

Another possibility is that the F-actin complex at the base of the head stabilizes and not only prevents further accumulation, but also a loss of accumulation. Ouyang et al. (2005) showed that the addition of jasplakinolide, which stabilizes F-actin through enhanced polymerization, resulted in a complete block of CaMKII accumulation into spines during LTP induction. This suggests that a physical barrier exists between the dendrite and spine head which must be depolymerized to allow translocation at activated spines. While F-actin exists throughout the spine, a stable pool with a slow rate of turnover with respect to other F-actin in the spine is localized to the base of the spine head (Honkura et al. 2008). During LTP induction, a pool of F-actin responsible for spine enlargement is created. Honkura et al. (2008) has shown that this pool had a lifetime of 2–15 min. Matsuzaki et al. (2004) and Harvey and Svoboda (2007) observed a peak in the volume enlargement of spines within several minutes of glutamate uncaging. After ~20 min the spine volume maintained a persistent enlargement which was less than peak volume, but ~50%–75% greater than basal volume. If the F-actin complex at the base of the head was also stabilized to its resting state, as was shown by Honkura et al. (2008), translocation both in and out of the spine would be inhibited. Our simulations show that the decay rate of CaMKII upon peak accumulation is ~20 min which predicts reversible translocation prior to stabilization, but an overall increase in CaMKII accumulation into the spine head upon F-actin stabilization.

Our results showed that monovalent high affinity binding alone cannot retain CaMKII in the spine long term. Also, monovalent high affinity binding cannot retain CaMKII in the short term without spine morphology creating a narrow escape problem. Either multivalent CaMKII binding sites at the PSD or the stabilization of F-actin at the base of the neck,

thereby creating a physical obstruction to diffusion, could explain accumulation into a time frame of hours. These mechanisms, generalized in our simulations, support the temporal windows of translocation found in the literature (Otmakhov et al. 2004; Zhang et al. 2008; Yamagata et al. 2009). In the future, constructing a detailed model of CaMKII accumulation during LTP induction will require more detailed kinetic data of PSD targets. More detailed imaging of the F-actin complex will also aid in the ability to reconstruct the complex in a 3D environment where its role as a physical barrier can be more extensively examined.

Supplementary Material

Refer to Web version on PubMed Central for supplementary material.

Acknowledgments

This work was supported by NIH grant NS038310.

References

Berezhkovskii AM, Barzykin AV, Zitserman VY. Escape from cavity through narrow tunnel. J Chem Phys. 2009; 130(24):245104. [PubMed: 19566185]

Biess A, Korkotian E, Holcman D. Diffusion in a dendritic spine: the role of geometry. Physical Review E-Statistical, Nonlinear and Soft Matter Physics. 2007; 76(2 Pt 1):021922.

Bloodgood BL, Sabatini BL. Neuronal activity regulates diffusion across the neck of dendritic spines. Science. 2005; 310(5749):866–869. [PubMed: 16272125]

Byrne MJ, Putkey JA, Waxham MN, Kubota Y. Dissecting cooperative calmodulin binding to CaM kinase II: a detailed stochastic model. Journal of Computational Neuroscience. 2009; 27(3):621–638. [PubMed: 19609660]

Byrne MJ, Waxham MN, Kubota Y. Cellular dynamic simulator: an event driven molecular simulation environment for cellular physiology. Neuroinformatics. 2010; 8(2):63–82. [PubMed: 20361275]

Dagdug L, Berezhkovskii AM, Makhnovskii YA, Zitserman VY. Transient diffusion in a tube with dead ends. The Journal of Chemical Physics. 2007; 127(22):224712. [PubMed: 18081419]

Goldstein B, Perelson AS. Equilibrium theory for the clustering of bivalent cell surface receptors by trivalent ligands. Application to histamine release from basophils. Biophysical Journal. 1984; 45(6): 1109–1123. [PubMed: 6204698]

Harris KM, Stevens JK. Dendritic spines of CA 1 pyramidal cells in the rat hippocampus: serial electron microscopy with reference to their biophysical characteristics. The Journal of Neuroscience. 1989; 9(8):2982–2997. [PubMed: 2769375]

Harvey CD, Svoboda K. Locally dynamic synaptic learning rules in pyramidal neuron dendrites. Nature. 2007; 450(7173):1173–1175. [PubMed: 18097394]

Holmes KC, Popp D, Gebhard W, Kabsch W. Atomic model of the actin filament. Nature. 1990; 347(6288):44–49. [PubMed: 2395461]

Honkura N, Matsuzaki M, Noguchi J, Ellis-Davies GC, Kasai H. The subspine organization of actin fibers regulates the structure and plasticity of dendritic spines. Neuron. 2008; 57(5):719–729. [PubMed: 18341992]

Ikawa T, Hoshino F, Watanabe O, Li Y, Pincus P, Safinya CR. Molecular scale imaging of F-actin assemblies immobilized on a photopolymer surface. Physical Review Letters. 2007; 98(1):018101. [PubMed: 17358507]

Kalantzis G, Kubota Y, Shouval HZ. Evaluating statistical methods used to estimate the number of postsynaptic receptors. Journal of Neuroscience Methods. 2009; 178(2):393–401. [PubMed: 19162073]

Kolodziej SJ, Hudmon A, Waxham MN, Stoops JK. Three-dimensional reconstructions of calcium/calmodulin-dependent (CaM) kinase IIalpha and truncated CaM kinase IIalpha reveal a unique organization for its structural core and functional domains. The Journal of Biological Chemistry. 2000; 275(19):14354–14359. [PubMed: 10799516]

Lee SJ, Escobedo-Lozoya Y, Szatmari EM, Yasuda R. Activation of CaMKII in single dendritic spines during long-term potentiation. Nature. 2009; 58(7236):299–304. [PubMed: 19295602]

Leonard AS, Lim IA, Hemsworth DE, Horne MC, Hell JW. Calcium/calmodulin-dependent protein kinase II is associated with the N-methyl-D-aspartate receptor. Proceedings of the National Academy of Sciences of the United States of America. 1999; 96(6):3239–3244. [PubMed: 10077668]

Lisman J, Schulman H, Cline H. The molecular basis of CaMKII function in synaptic and behavioural memory. Nature Reviews Neuroscience. 2002; 3(3):175–190.

Majewska A, Tashiro A, Yuste R. Regulation of spine calcium dynamics by rapid spine motility. The Journal of Neuroscience. 2000; 20(22):8262–8268. [PubMed: 11069932]

Matsuzaki M, Honkura N, Ellis-Davies GC, Kasai H. Structural basis of long-term potentiation in single dendritic spines. Nature. 2004; 429(6993):761–766. [PubMed: 15190253]

Merrill MA, Chen Y, Strack S, Hell JW. Activity-driven postsynaptic translocation of CaMKII. Trends in Pharmacological Sciences. 2005; 26(12):645–653. [PubMed: 16253351]

Neuman SP, Tartakovsky DM. Perspective on theories of non-Fickian transport in heterogeneous media. Advances in Water Resources. 2009; 32(5):670–680.

Ohta Y, Nishida E, Sakai H. Type II Ca2+/calmodulin-dependent protein kinase binds to actin filaments in a calmodulin-sensitive manner. FEBS Letters. 1986; 208(2):423–426. [PubMed: 3780978]

Okamoto K, Narayanan R, Lee SH, Murata K, Hayashi Y. The role of CaMKII as an F-actin-bundling protein crucial for maintenance of dendritic spine structure. Proceedings of the National Academy of Sciences of the United States of America. 2007; 104(15):6418–6423. [PubMed: 17404223]

Otmakhov N, Tao-Cheng JH, Carpenter S, Asrican B, Dosemeci A, Reese TS, et al. Persistent accumulation of calcium/calmodulin-dependent protein kinase II in dendritic spines after induction of NMDA receptor-dependent chemical long-term potentiation. The Journal of Neuroscience. 2004; 24(42):9324–9331. [PubMed: 15496668]

Ouyang Y, Wong M, Capani F, Rensing N, Lee CS, Liu Q, et al. Transient decrease in F-actin may be necessary for translocation of proteins into dendritic spines. The European Journal of Neuroscience. 2005; 22(12):2995–3005. [PubMed: 16367766]

Robison AJ, Bartlett RK, Bass MA, Colbran RJ. Differential modulation of Ca2+/calmodulin-dependent protein kinase II activity by regulated interactions with N-methyl-D-aspartate receptor NR2B subunits and alpha-actinin. The Journal of Biological Chemistry. 2005; 280(47):39316–39323. [PubMed: 16172120]

Sanabria H, Digman MA, Gratton E, Waxham MN. Spatial diffusivity and availability of intracellular calmodulin. Biophysical Journal. 2008; 95(12):6002–6015. [PubMed: 18820232]

Sanabria H, Swulius MT, Kolodziej SJ, Liu J, Waxham MN. βCaMKII regulates actin assembly and structure. The Journal of Biological Chemistry. 2009; 284(15):9770–9780. [PubMed: 19208632]

Santamaria F, Wils S, De Schutter E, Augustine GJ. Anomalous diffusion in Purkinje cell dendrites caused by spines. Neuron. 2006; 52(4):635–648. [PubMed: 17114048]

Saxton MJ. Anomalous diffusion due to obstacles: a Monte Carlo study. Biophysical Journal. 1994; 66(2 Pt 1):394–401. [PubMed: 8161693]

Saxton MJ. Anomalous diffusion due to binding: a Monte Carlo study. Biophysical Journal. 1996; 70(3):1250–1262. [PubMed: 8785281]

Shen K, Meyer T. Dynamic control of CaMKII translocation and localization in hippocampal neurons by NMDA receptor stimulation. Science. 1999; 284(5411):162–166. [PubMed: 10102820]

Shen K, Teruel MN, Connor JH, Shenolikar S, Meyer T. Molecular memory by reversible translocation of calcium/calmodulin-dependent protein kinase II. Nature Neuroscience. 2000; 3(9): 881–886.

Strack S, Colbran RJ. Autophosphorylation-dependent targeting of calcium/calmodulin-dependent protein kinase II by the NR2B subunit of the N-methyl- D-aspartate receptor. The Journal of Biological Chemistry. 1998; 273(33):20689–10692. [PubMed: 9694809]

Strack S, Robison AJ, Bass MA, Colbran RJ. Association of calcium/calmodulin-dependent kinase II with developmentally regulated splice variants of the postsynaptic density protein densin-180. The Journal of Biological Chemistry. 2000; 275(33):25061–25064. [PubMed: 10827168]

Sykova E, Nicholson C. Diffusion in brain extracellular space. Physiological Reviews. 2008; 88(4): 1277–1340. [PubMed: 18923183]

Walikonis RS, Jensen ON, Mann M, Provance DW Jr, Mercer JA, Kennedy MB. Identification of proteins in the postsynaptic density fraction by mass spectrometry. The Journal of Neuroscience. 2000; 20(11):4069–4080. [PubMed: 10818142]

Yamagata Y, Kobayashi S, Umeda T, Inoue A, Sakagami H, Fukaya M, et al. Kinase-dead knock-in mouse reveals an essential role of kinase activity of Ca2+/calmodulin-dependent protein kinase IIalpha in dendritic spine enlargement, long-term potentiation, and learning. The Journal of Neuroscience. 2009; 29(23):7607–7618. [PubMed: 19515929]

Zhang YP, Holbro N, Oertner TG. Optical induction of plasticity at single synapses reveals input-specific accumulation of αCaMKII. Proceedings of the National Academy of Sciences of the United States of America. 2008; 105(33):12039–12044. [PubMed: 18697934]

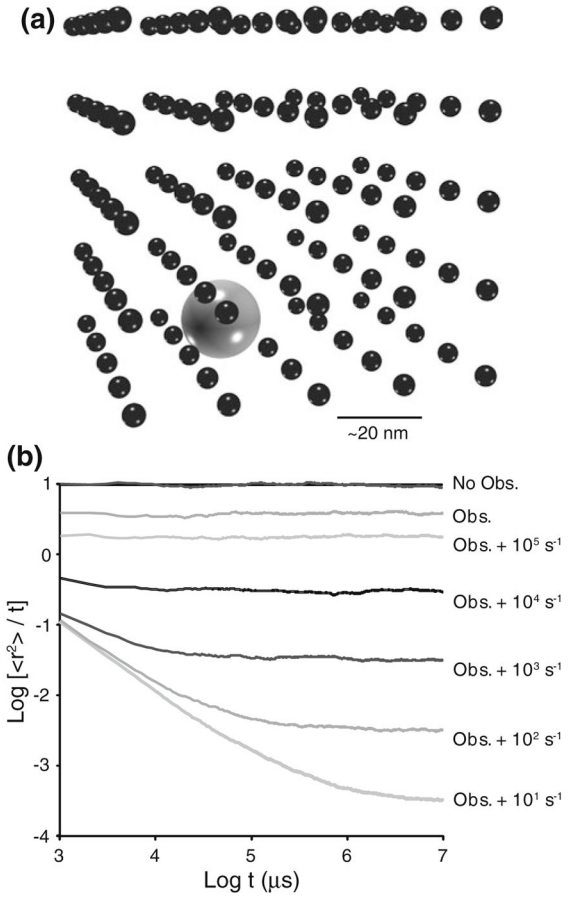

Fig. 1.

The impact of obstacles with and without binding. (**a**) The simulation environment was constructed with a cube of 100 nm sides and had a periodic boundary. Obstacles (*black*) were placed on a regular lattice with 20 nm spacing. CaMKII (grey) was randomly placed in the environment. (**b**) Simulations were run for 1 s and repeated 500 times and the averaged behavior for each condition is shown. For diffusion in the absence and presence of obstacles (at this density) without binding sites, the MSD was proportional to time. Anomalous (sub-) diffusion will show a deviation from this horizontal straight line. In the presence of obstacles with binding sites, we started to observe anomalous diffusion with a dissociation rate of 10^4 s^{-1} which became more obvious as the dissociation rate slowed. Note that the diffusion began as anomalous, but relaxed back to normal diffusion (*horizontal straight line*) within 0.5 s. Anomalous diffusion in all cases was transitional; however, the duration of the transition to normal diffusion increased as the dissociation rate was reduced

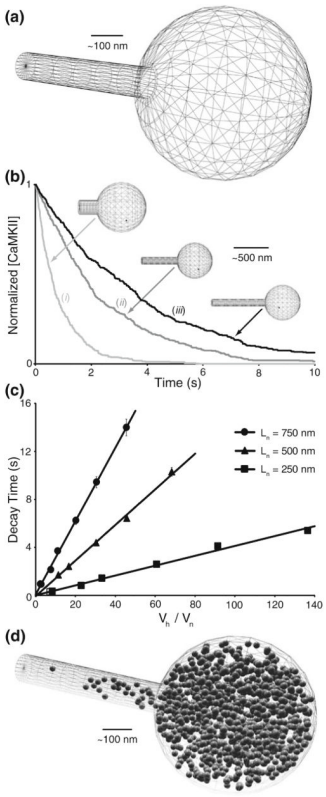

Fig. 2.

Narrow escape problem. (**a**) Spine morphology was represented as a cylinder attached to a sphere. (**b**) Exit time of CaMKII shown from three morphologies with varied head and neck radii and neck lengths of 250 nm (i), 500 nm (ii) and 750 nm (iii). The spine used for trace i had a volume ratio 37% greater than spine ii and 105% greater than spine iii yet had the fastest decay rate as a result of the smallest L_n. (**c**) Decay time out of the spine was proportional to the ratio of the head volume and neck volume (V_h/V_n) given a fixed neck length (L_n). Three values for L_n were used, 250, 500 and 750 nm. The slope of each data set was approximately equal to L_n^2/D as predicted by Eq. (2). A spine of average dimensions (r_h=300 nm, r_n=75 nm, L_n=500 nm) had a decay rate of ~4 s. (**d**) A single CaMKII was placed at the center of the spine head and allowed to diffuse until it exited the spine (after 2.87 s). Here we show its position every 2.5 ms to demonstrate that CaMKII visits every section of the spine head during the time it was trapped. In this figure, CaMKII does not appear to have travelled much into the neck; however, CaMKII entered the neck then reentered the head five times (the sixth entry into the neck finally led to escape)

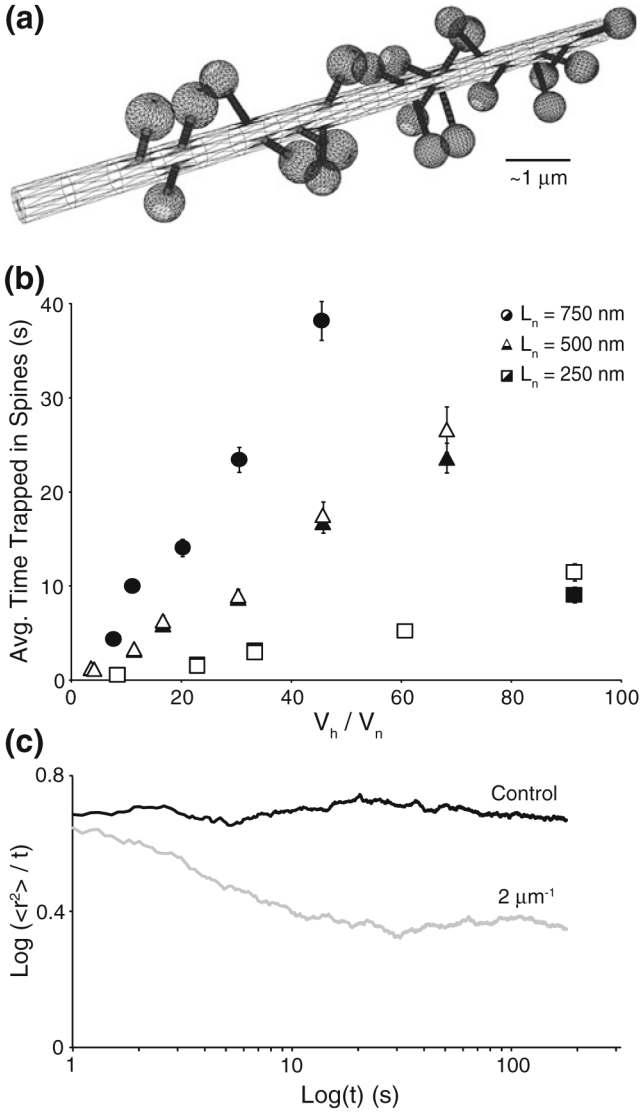

Fig. 3.

Trapping of dendritic CaMKII. (**a**) A section of dendrite was created as a cylinder 10 μm in length and a radius of 200 or 400 nm. Spine morphology was created in the same manner as the narrow escape problem. 20 spines were distributed along the dendrite to give a density of 2 μm^{-1}. For each unique geometry used, 10 different environments were generated with uniformly distributed spine locations. Simulations were run for 180 s. (**b**) The average time CaMKII was trapped in the spines was proportional to V_h/V_n given a fixed L_n. The radius of the dendrite had no effect on the average trapping time. Filled shapes indicate a 200 nm dendrite radius and open shapes indicate 400 nm radius. (**c**) A 150 μm section of dendrite was created with CaMKII initiated at the center. Two cases were evaluated, a control environment with no spines and an environment with a spine density of 2 spines per μm. The simulation was run for 180 s while tracking the mean squared displacement. The control case showed free diffusion while the spine case showed anomalous diffusion for 20 s, then became free. 1000 trials were performed and averaged in each case

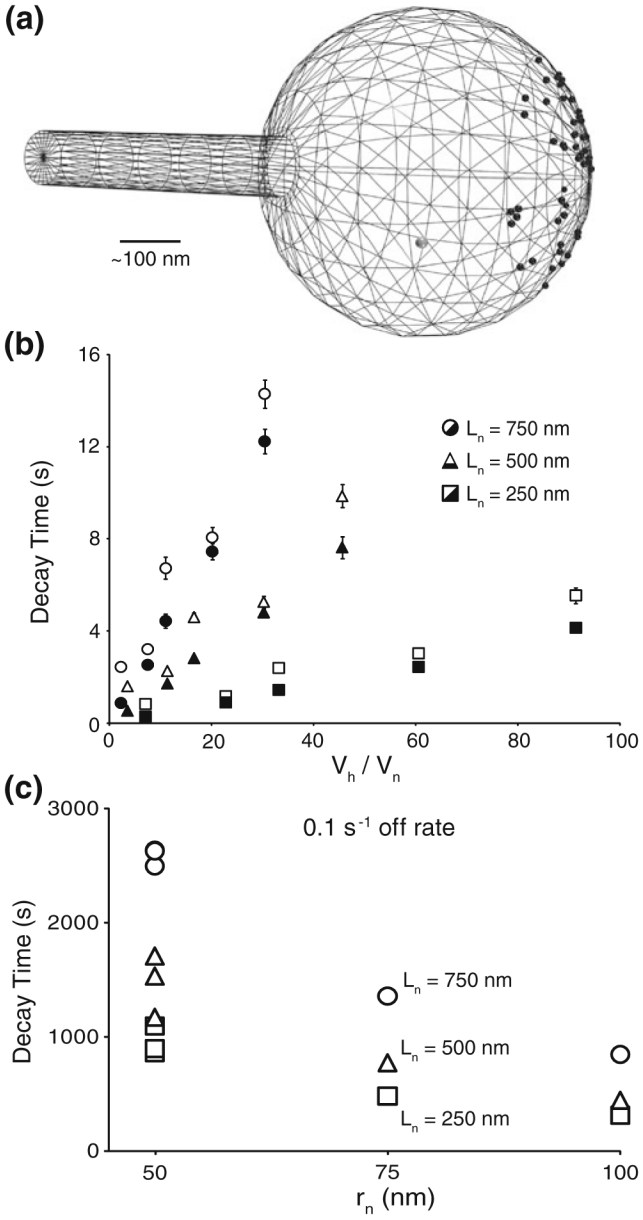

Fig. 4.

Narrow escape problem with a high binding sites in the PSD (**a**) A PSD-like structure was added to the narrow escape problem and targets of varying affinity were distributed about the PSD. (**b**) As experienced with the narrow escape problem, when L_n was fixed, decay rates were proportional to V_h/V_n. The decay rates were slower than the narrow escape problem by 10.9 and 76.9% when using PSD dissociation rates of 10^4 and 10^2 s^{-1}, respectively. The goodness of fit for the linear regression on the higher affinity case was 4.1% less than the lower affinity case. As higher affinity to PSD targets is used, the decay time proportional to the volume ratios breaks down. (**c**) For the high affinity case (0.1 s^{-1} dissociation rate), L_n was no longer the dominating factor for decreasing the decay rate. R_n, varied at 50, 75 and 100 nm, became the dominant geometry associated factor that controlled the decay time

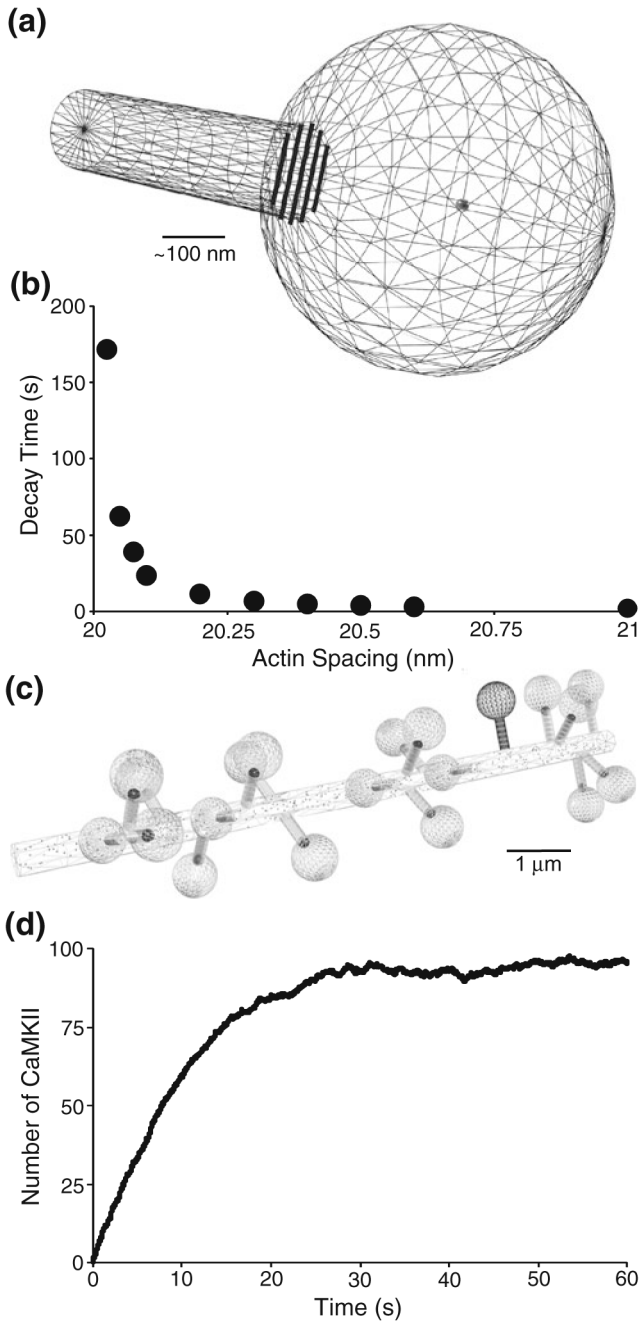

Fig. 5.

F-actin as a passive block to diffusion. (**a**) Parallel tracks of cylindrical F-actin were added to the base of the spine head with otherwise average dimensions. F-actin was placed with spacing from 20.025 to 24 nm. (**b**) Decay rates out of the spine exhibited a sharp transition between blocked diffusion and fast diffusion out of the spine. A spacing of 20.2 nm had a decay rate faster than that of a spine with a large (but common) V_h/V_n ratio with no diffusion constraints other than morphology. Spacing greater than 24 nm showed little change from the decay rate with no F-actin present. (**c**) The trapping simulation was modified such that 0.5 μM of CaMKII were added to the dendrite and all but one of the spines had a 100% physical block to the diffusing molecules. In these simulations, we used

average spine/neck geometries and included PSDs with high affinity (1 s^{-1} dissociation rate) binding targets to each spine. (**d**) The CaMKII population of the unblocked spine was recorded to track the rate of translocation. The time until the half-maximal concentration of accumulation in the spine was 7.25 s

Table 1

Exponential fits for narrow escape from spine with PSD (10–1 dissociation rate)

L_n	r_h (nm)	r_n	V_h/V_n	A_f(%)	τ_f(S)	A_s(%)	τ_s(S)
250	150	50	7.2	54	40.6	46	862.6
250	350	100	22.9	50	15.8	50	318.5
250	250	50	33.3	43	59.7	57	903.0
250	400	75	60.7	43	31.0	57	489.1
250	350	50	91.5	46	60.0	54	1097.8
500	150	50	3.6	40	41.9	60	1174.1
500	350	100	11.4	42	40.3	58	444.7
500	250	50	16.7	37	60.7	63	1536.3
500	400	75	30.3	43	70.6	57	774.3
500	350	50	45.7	29	76.0	71	1712.5
750	150	50	2.4	56	151.7	44	2497.4
750	350	100	7.6	63	123.7	37	847.9
750	250	50	11.1	46	216.2	54	2634.0
750	400	75	20.2	58	271.8	42	1358.2
750	350	50	30.5	45	223.1	55	2627.0